International Journal of Electrospun Nanofibers and Applications, Vol. 3, No. 2 (July-December, 2017)
ISSN : 0973-628X

Structure and Magnetic Properties of Electrospun Nickel Ferrite ($NiFe_2O_4$) Nanofibers

Wichaid Ponhan[a] & Santi Maensiri[a,b,*]

[a]*Small & Strong Materials Group (SSMG), Department of Physics, Faculty of Science Khon Kaen University, Khon Kaen, 40002, Thailand*

[b]*Integrated Nanotechnology Research Center (INRC), faculty of Science Khon Kaen University, Khon Kaen, 40002, Thailand*

Abstract: *This paper describes the fabrication of nickel ferrite ($NiFe_2O_4$) nanofibers by electrospinning method using a solution that contained poly(vinyl pyrrolidone) (PVP) and cheap Ni and Fe nitrates as alternative metal sources. The as-spun and calcined $NiFe_2O_4$/PVP composite samples were characterized by TG-DTA, X-ray diffraction, FT-IR, SEM and TEM, respectively. After calcination of the as-spun $NiFe_2O_4$/PVP composite nanofibers (fiber size of 321 ± 66 nm in diameter) at 500 °C in air for 3 h, $NiFe_2O_4$ nanofibers of 74 ± 13 nm in diameter having well-developed spinel structure were successfully obtained. The crystal structure and morphology of the nanofibers were influenced by the calcination temperature. After calcination at 600, and 700 °C, the nature of nanofibers was changed, which may be due to the reorganization of the $NiFe_2O_4$ structure at high temperature. A structure of packed particles or crystallites was prominent. Crystallite size of the nanoparticles contained in nanofibers increases from 9 nm to 27 nm with increasing calcination temperature between 500°C and 600°C. Room temperature magnetization results showed a ferromagnetic behavior of the calcined $NiFe_2O_4$ / PVP composite nanofibers, having their hysteresis loops in the field range of ± 2000 Oe. The specific saturation magnetization (Ms) values of 28.8, 31.9, and 35.5 emu/g were observed for the $NiFe_2O_4$/PVP composite nanofibers calcined at 500, 600, and 700 °C, respectively.*

Keywords: *Nickel ferrite; Nanofibers; Electrospinning; Transmission electron microscopy; X-ray diffraction; Magnetic properties; Nanofabrication*

1. INTRODUCTION

Nickel ferrite ($NiFe_2O_4$) is one of the most important spinel ferrites. It has an inverse spinel structure showing ferrimagnetism that originates from magnetic moment of anti-parrallel spins between Fe^{3+} ions at tetrahedral sites and Ni^{2+} ions at octahedral sites [1]. $NiFe_2O_4$ is technologically important and has been used in many applications including ferrofluids [2], hyperthermia agent in biomedicine [3], catalysts [4], microwave devices [5], gas sensors [6], magnetic carriers for drug delivery [7], anodic material in lithium ion batteries [8] etc. Recently, nanocrystalline magnetic materials have received more and more attention due to their novel material properties that are significantly different

corresponding author: sanmae@kku.ac.th; santimaensiri@gmail.com

from those of their bulk counterparts [9]. Various methods have been developed to synthesize nanocrystalline $NiFe_2O_4$, including sonochemical process [10], citrate precursor techniques [11], coprecipitation [12], mechanical alloying [13], sol–gel [14], pulsed wire discharge [15], shock wave [16], reverse micelle [17], hydrothermal [18], ultrasonically assisted hydrothermal process [19], and egg white solution route [20]. The ordered magnetic materials such as nanorods and nanowires have currently attracted a great interest due to their enhanced magnetic properties [21,22]. Nanofiberization of magnetic materials would also be of great interest and will expand their technological application in many areas including nanocomposites, nanosensors, nano-electronics and photonics.

Electrospinning represents a simple and convenient method for preparing polymer fibers and ceramic fibers with both solid and hollow interiors that are exceptionally long in length, uniform in diameter ranging from tens of nanometers to several micrometers, and diversified in compositions [23-26]. In an electrospinning process [27-30], an electrical potential is applied between a droplet of a polymer solution held at the end of the nozzle of the spinneret and a grounded target. When the applied electric field overcomes the surface tension of the droplet, a charged jet of polymer solution is ejected. The route of the charged jet is controlled by the electric field. The jet exhibits bending instabilities caused by repulsive forces between the charges carried with the jet. The jet extends through spiralling loops. As the loops increase in diameter the jet grows longer and thinner until it solidifies or is collected on the target. Some novel metal oxide nanofibers e.g. TiO_2 [31] and ZnO [32], and oxide ceramic compounds e.g. $Pb(Zr_{0.52}Ti_{0.48})O_3$ [33], $NaCo_2O_4$ [34], and $Ba_{0.6}Sr_{0.4}TiO_3$ [35] have been successfully prepared by electrospinning process followed by calcination at high temperature. Electrospinning of $NiFe_2O_4$ nanofibers was first reported by Li *et al.* [36]. In their study polycrystalline nanofibers of $NiFe_2O_4$ with an average diameter of 46 nm were prepared by electrospinning a solution that contained poly(vinyl pyrrolidone) (PVP) and alkoxide precursors to nickel and iron oxides, followed by calcination at 550 °C in air. However, metal alkoxide precursors used in their study are expensive and may not be suitable for large scale production. Moreover, solution preparation for electrospinning must be carried out in glove-box to prevent oxidation of the metal alkoxide precursors. Therefore, the use of alternative precursor without the need of glove-box or special procedures would be preferable.

This paper reports on the fabrication of $NiFe_2O_4$/PVP composite nanofibers by electrospinning using a solution that contained poly(vinyl pyrrolidone) and cheap Ni and Fe nitrates as alternative metal sources. The $NiFe_2O_4$ nanofibers were obtained after calcination of $NiFe_2O_4$/PVP composite nanofibers at high temperatures. The fabricated $NiFe_2O_4$/PVP and $NiFe_2O_4$ samples were characterized by TG-DTA, XRD, FTIR, SEM, and TEM. The magnetic properties of fabricated $NiFe_2O_4$/PVP and $NiFe_2O_4$ samples were investigated using a vibrating sample magnetometer (VSM) at room temperature (20 °C). The effects of calcination temperature on morphology, structure, and magnetic properties of the fabricated $NiFe_2O_4$/PVP composite samples were also studied.

2. MATERIALS AND METHODS

In this study, $Ni(NO_3)_2.6H_2O$ (99.99% purity, Kanto Chemicals, Japan), $Fe(NO_3)_3.9H_2O$ (99.99% purity, Kanto Chemicals, Japan) and polyvinyl pyrrolidone (PVP) (M_n = 1,300,000, Aldrich), N, N dimetylformamide (DMF) (99.8% purity, Fluka, Switzerland), acetic acid (BDH, 100%) and ethanol (BDH, 100%) were used as the starting chemicals. In the preparation of the solution for electrospinning, we used a solution that contained poly(vinyl pyrrolidone) mixed with $Ni(NO_3)_2.6H_2O$ and $Fe(NO_3)_3.9H_2O$. A PVP/ethanol solution was prepared using 1.0 g PVP dissolved into 9 ml ethanol. A metal nitrates/DMF solution was prepared by dissolving 0.01 mol $Ni(NO_3)_2.6H_2O$ and 0.02 mol $Fe(NO_3)_3.9H_2O$) in 10 ml of DMF and stirred for 5 h. Subsequently, the metal nitrates/DMF solution (4 ml) was added slowly to the PVP/ethanol solution (50 ml) under vigorous stirring at 300 K for 5 h to obtain a well-dissolved solution. This final solution was used for electrospinning.

The prepared polymer solution was loaded into a plastic syringe equipped with a 22-gauge needle made of stainless steel. The electrospinning process was carried out using our home-made electrospinning system. The schematic diagram of electrospinning process is shown in Figure 1. The needle was connected to a high-voltage supply and for each solution the voltage of 15 kV was applied. The solution was fed at a rate of 1.0 mL/h using a motor syringe pump. A piece of flat aluminum foil was placed 15 cm below the tip of the needle, and used to collect the nanofibers. All electrospinning processes were carried out at room temperature.

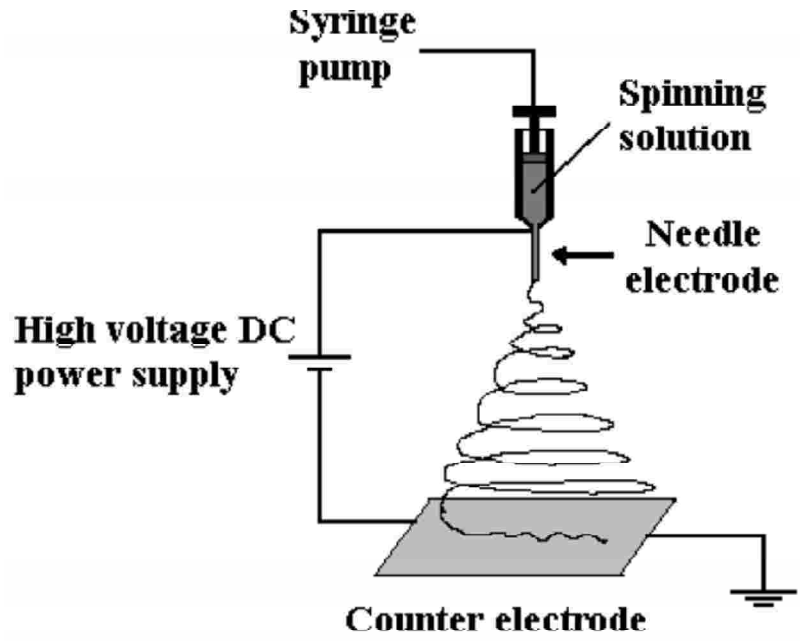

Figure 1: Schematic Diagram of Electrospinning Set up

The as-spun $NiFe_2O_4$/PVP composite nanofibers were subjected to thermogravimetric-differential thermal analysis (TG-DTA) using Pyris Diamond TG/DTA (PerkinElmer Instrument, USA). This was done to determine the temperatures of possible decomposition and crystallization (or phase changes) of the as-spun nanofibers. The analyses were performed with a heating rate of 5 °C/min in static air up to 1000 °C. The composite nanofibers were calcined at 500, 600, and 700 °C for 2 h in air in box furnace (Lenton Furnaces, U.K.), using heating and cooling rates of 5 °C/min. The final products obtained were light black $NiFe_2O_4$ samples. The as spun and calcined composite nanofibers were characterized by means of X-ray diffraction (XRD) using CuK_α radiation with λ = 0.15418 nm (PW3040 mpd control, The Netherlands), FT-IR spectroscopy (Spectrum One FT-IR Spectrometer, PerkinElmer Instruments, USA), scanning electron microscopy (SEM) (Hitachi FE-SEM S-4700, Japan) and transmission electron microscopy (TEM) (JEOL TEM 2010, Japan). The average diameters of the as-spun and calcined composite nanofibers were determined from about 300 measurements. The magnetic properties of the calcined samples were examined at room temperature (20 °C) using a vibrating sample magnetometer (VSM) (Lake Shore VSM 7403, USA).

3. RESULTS AND DISCUSSION

The TG curve in Figure 2 shows a minor weight loss step from 30 °C up to about 200 °C and a major weight loss step from 200 °C up to about 320 °C. Above 320 °C, no further weight loss was observed up to 1000 °C. The minor weight loss was related to the loss of moisture and trapped solvent (water, ethanol and carbon dioxide) in the as-spun nanofibers while the major weight loss was due to the combustion of organic PVP matrix. On the DTA curve, a main exothermic peak was observed at ~320 °C, suggesting the

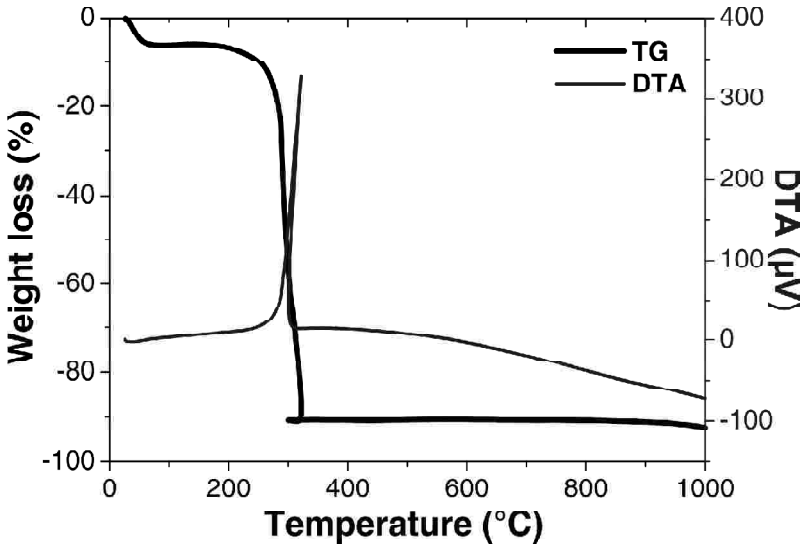

Figure 2: TG-DTA Curves of Thermal Decomposition of the As-spun $NiFe_2O_4$/PVP Composite Nanofibers at a Heating Rate of 5 °C/min in Static Air

thermal events related to the decomposition of Ni and Fe nitrates along with the degradation of PVP by a dehydration on the polymer side chain, which was confirmed by a dramatic weight loss in TG curve at the corresponding temperature range (250-320 °C). The plateau formed between 320 and 1000 °C on the TG curve indicated the formation of nanocrystalline $NiFe_2O_4$ as the decomposition product [20, 31, 35], as confirmed by selected area electron diffraction (SAED) in TEM, XRD and FT-IR analyses discussed in details later.

The morphology of the as-spun and calcined $NiFe_2O_4$/PVP composite nanofibers was revealed by SEM. Figure 3 shows the SEM micrographs of the as-spun and calcined $NiFe_2O_4$/PVP composite nanofibers. The respective diameter histograms of the as-prepared and 500 °C-calcined $NiFe_2O_4$/PVP composite nanofibers are also shown in the insets of Figures 3a and 3b. The as-spun composite nanofibers appeared quite smooth due to the amorphous nature of $NiFe_2O_4$/PVP composite (Figure 3a). Each individual nanofiber was quite uniform in cross section, and the average diameter of the fibers was 321 66 nm. The PVP was selectively removed by calcination of the as-spun composite nanofibers in air at above 500 °C. All the calcined nanofibers formed a structure of packed particles or crystallites. These changes in the morphology are related to a dramatic change in crystal structure as observed in electrospun $NaCo_2O_4$ [34], and $Ba_{0.6}Sr_{0.4}TiO_3$ [35]. The nanofibers calcined at 500 °C remained as continuous structures (Figure 3b), and their diameters appeared to be decreased to 74 ± 13 nm. The reduction in size of the nanofibers should be attributed to the loss of PVP from the nanofibers and the crystallization of $NiFe_2O_4$. After calcination at 600, and 700 °C, the nature of nanofibers changed, which may be due to the reorganization of the $NiFe_2O_4$ structure at high temperature. A structure of packed particles or crystallites was prominent.

The detailed morphology and crystalline structure of the calcined $NiFe_2O_4$/PVP composite nanofibers were further investigated by TEM. Figure 4a-c show TEM bright field images with corresponding selected-area electron diffraction (SAED) patterns of the $NiFe_2O_4$/PVP composite nanofibers calcined in air for 3 h at different temperatures. It is clearly seen from the TEM bright-field images (Figure 4) that the morphology and size of the materials were significantly affected by the calcination temperature. The calcined composite nanofibers consisted of packed $NiFe_2O_4$ particles or crystallites. The particle sizes of nanofibers calcined at 500, 600, and 700 °C were ~ 10-15, 20-30, and 30-80 nm in diameter, respectively. It is worth noting that the particle sizes of $NiFe_2O_4$ contained in the calcined $NiFe_2O_4$/PVP composite nanofibers are quite uniform. This might have resulted from the rates of hydrolysis involved in the fabrication process that the water required for the hydrolysis of metal precursors was supplied by the moisture in air [36]. Since the electrospun fibers were very small in diameter, the moisture could quickly diffuse into the fibers, causing a rapid and uniform hydrolysis of the metal precursors. The corresponding selected-area electron diffraction (SAED) patterns (Figure 4) of all the $NiFe_2O_4$/PVP composite nanofibers show spotty ring patterns without any additional diffraction spots and rings of second phases, revealing their crystalline spinel structure. Measured interplanar spacings (d_{hkl}) from selected-area electron diffraction patterns in Figure 4 are in good agreement with the values in the standard data (JCPDS:

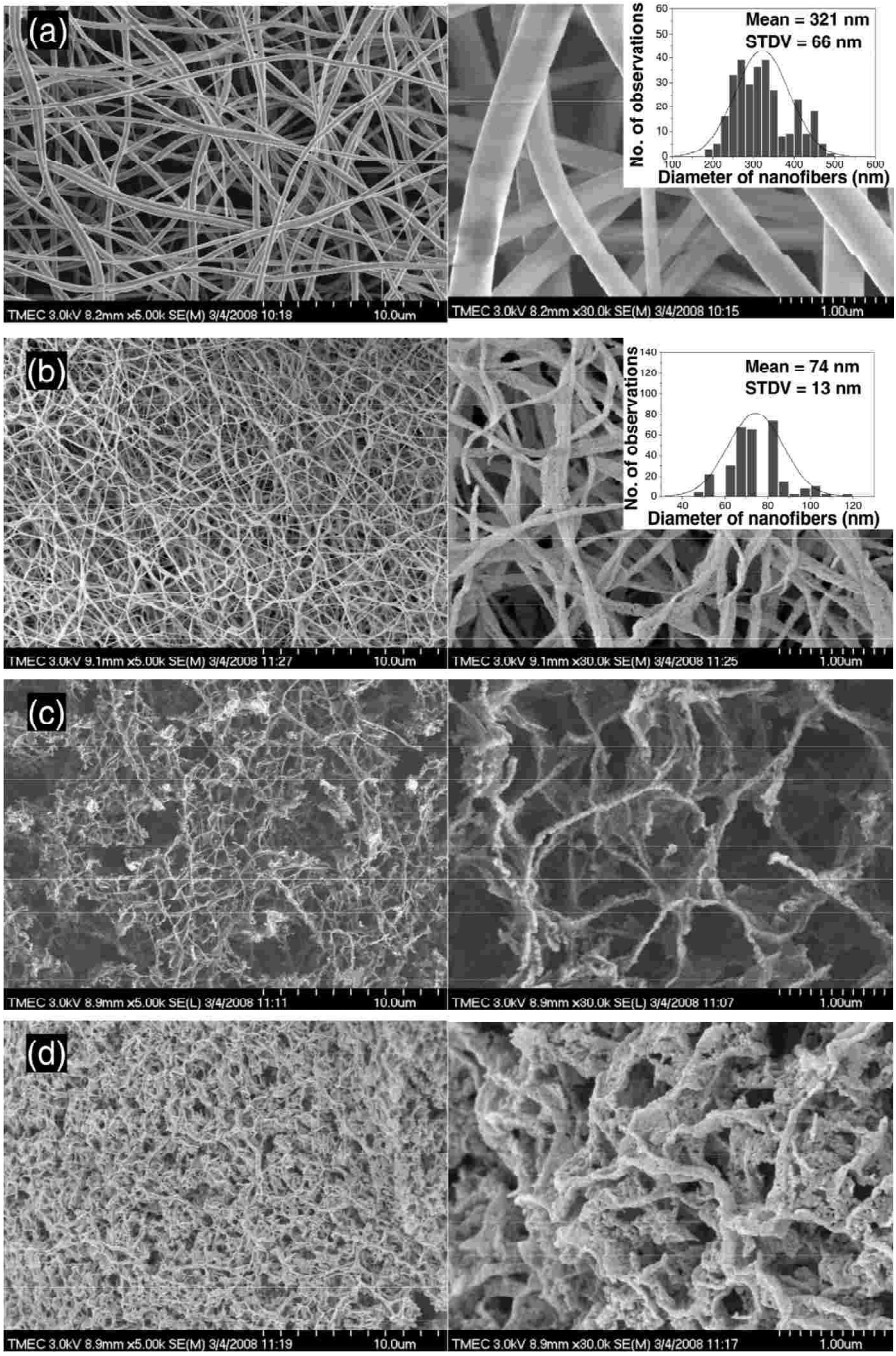

Figure 3: SEM Micrographs of the As-spun $NiFe_2O_4$/PVP Composite Sample and $NiFe_2O_4$/PVP Composite Samples Calcined in air at Different Temperatures for 3 h. (a) As-spun, (b) 500 °C, (c) 600 °C, and (d) 700 °C

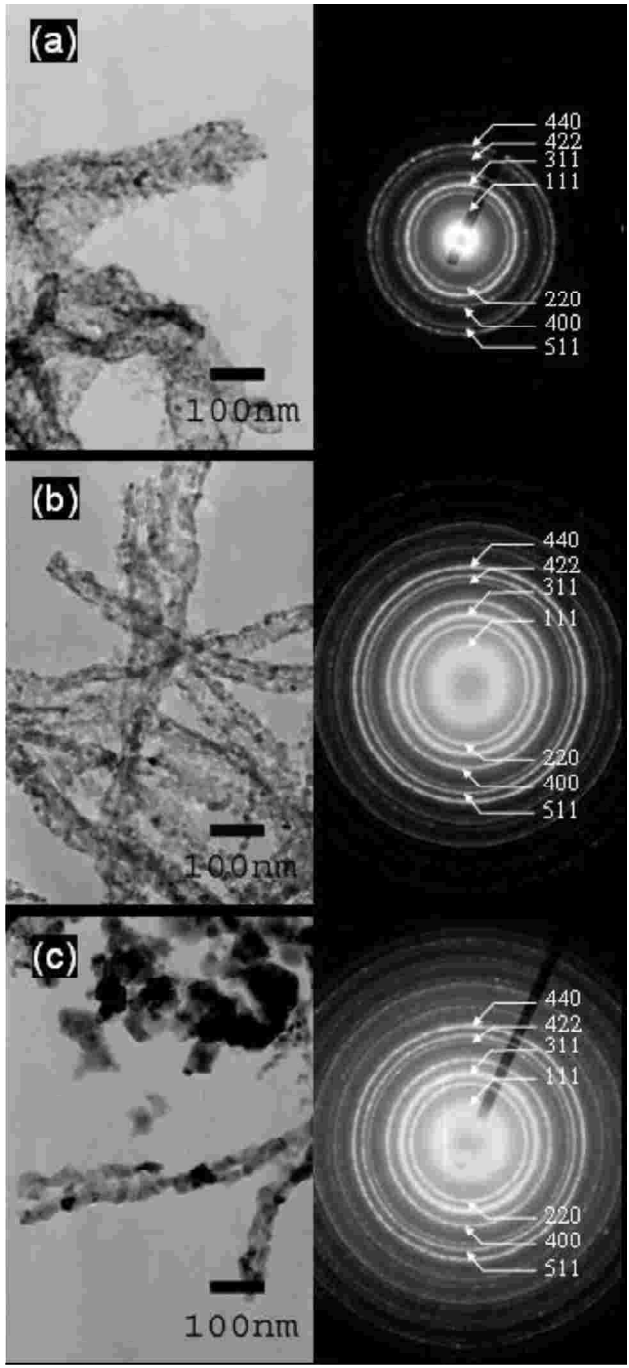

Figure 4: TEM Images with Corresponding Selected Area Electron Diffraction Patterns of the $NiFe_2O_4$/PVP Composite Samples Calcined in Air for 3 h at Different Temperatures. (a) 500 °C, (b) 600 °C, and (c) 700 °C

10-0325). The diffraction rings are identified as the (111), (220), (311), (400), (422), (511) and (440) planes. This concurs with the results of XRD presented in Figure 5.

The XRD patterns of the calcined $NiFe_2O_4$/PVP composite nanofibers are shown in Figure 5. All of the main peaks are indexed as the $NiFe_2O_4$ with inverse spinel structure as shown in the standard data (JCPDS: 10-0325). It is clearly seen that the reflection peaks become slightly sharper and narrower along with the increasing of calcination temperatures, indicating the enhancement of crystallinity. The average crystallite sizes of $NiFe_2O_4$ samples were calculated from X-ray line broadening of the reflections of (311) using Scherrer's equation (i.e. $D = K\lambda / (\beta \cos\theta)$, where λ is the wavelength of the X-ray radiation, K is a constant taken as 0.89, θ is the diffraction angle and β is the full width at half maximum (*FWHM*) [37]), and were found to be 9, 21 and 27 nm for the samples of $NiFe_2O_4$/PVP composite nanofibers calcined at 500, 600, and 700 °C, respectively. The lattice parameters a calculated from the XRD spectra were 0.8338 ± 0.0001, 0.8340 ± 0.0001, and 0.8342 ± 0.0001 nm for the samples of $NiFe_2O_4$/PVP composite nanofibers calcined at 500, 600, and 700 °C, respectively. The values of the lattice parameter a slightly increase with increasing calcination temperature and are close to (within 0.0003 nm) that reported for $NiFe_2O_4$ (a = 0.8339 nm) in the standard data (JCPDS: 10-0325). The crystallite sizes and lattice parameters are also summarized in Table 1.

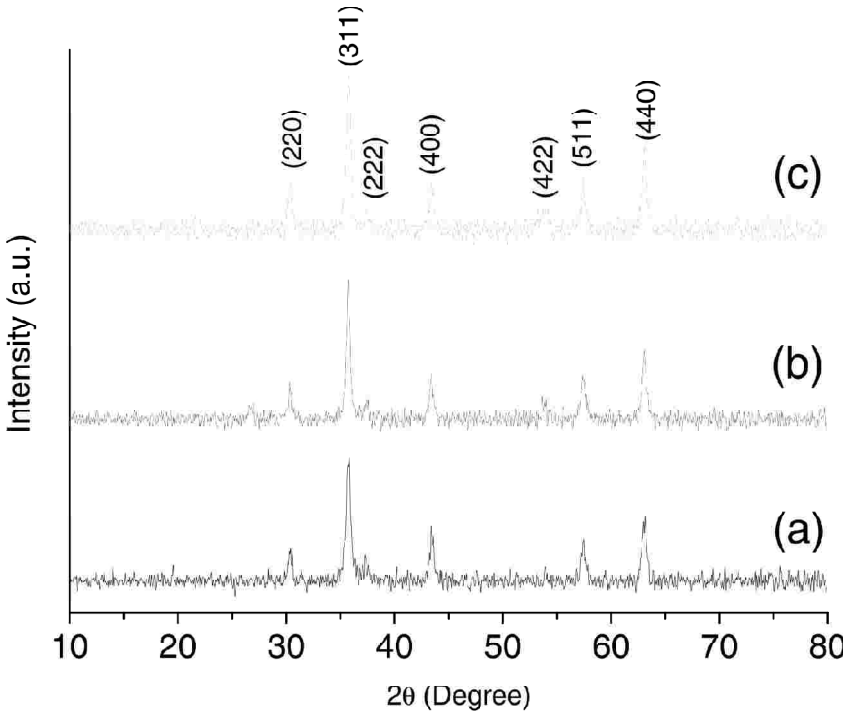

Figure 5: XRD Patterns of the $NiFe_2O_4$/PVP Composite Samples Calcined in Air for 3 h at Different Temperatures. (a) 500 °C, (b) 600 °C, and (c) 700 °C

Table 1
Average Crystal Sizes from XRD, Spinel Lattice Parameter a Calculated from XRD Spectra, the Specific Magnetization (M_s), Remnant Magnetization (M_r), the Ratio of the Ratio of Remnant Magnetization to Bulk Saturation Magnetization (M_r/M_s), and Coercive Forces (H_c) of the $NiFe_2O_4$/PVP Composite Samples Calcined in Air at 500, 600, and 700 °C for 3 h

$NiFe_2O_4$ sample	*Average crystallite size from XRD (nm)*	*Spinel lattice parameter a (nm)*	*M_s (emu/g) at 10kOe*	*M_r (emu/g)*	*M_r/M_s*	*H_c (Oe)*	*Estimated region of hysteresis (Oe)*
Calcined at 500 °C	9	0.8338 ± 0.0001	28.8	4.4	0.152	130.5	± 2000
Calcined at 600 °C	21	0.8340 ± 0.0001	31.9	4.5	0.141	114.0	± 2000
Calcined at 700 °C	27	0.8342 ± 0.0001	35.5	6.7	0.188	13.5	± 2000

The formation of spinel $NiFe_2O_4$ structure in the calcined $NiFe_2O_4$/PVP composite nanofibers was further supported by FT-IR spectra (Figure 6). Here we consider two ranges of the absorption bands: 4000-1000 cm^{-1} and 1000-370 cm^{-1} as suggested by previously published work [38-40]. In the range of 4000-1000 cm^{-1}, vibrations of CO_3^{2-}, NO_3^- and moisture were observed. The intensive broadband at ~3432 cm^{-1} and the less intensive band at ~ 1617 cm^{-1} are due to O-H stretching vibration interacting through H bonds. Traces of adsorbed or atmospheric CO_2 are evidenced by the very small absorption peak around 2352 cm^{-1}. The ν (C = O) stretching vibration of the carboxylate group (CO_2^-) is observed around 1380 $cm^{-1}$and the band at ~1008 cm^{-1} corresponds to nitrate ions traces. Therefore, the CO_3^{2-} and CO_2^- vibrations disappeared when calcination temperature was increased. In the range of 1000–400 cm^{-1}, a main metal–oxygen band at ~595 cm^{-1} was observed in the FTIR spectra of all of the calcined $NiFe_2O_4$/PVP composite nanofibers. This band is usually assigned to the vibration of ions in the crystal lattices [41]. The band at ~595 cm^{-1}coresponds to intrinsic stretching vibration of the metal at the tetrahedral site (Fe ↔ O) [42, 43].

The specific magnetization curves of the calcined $NiFe_2O_4$/PVP composite nanofibers obtained from room temperature VSM measurement are shown in Figure 7. These curves are typical for a soft magnetic material and indicate hysteresis ferromagnetism in the field range of ± 2000 Oe while outside this range the specific magnetization increases with increasing field and saturates in the field range investigated (± 10 kOe). The specific saturation magnetization (M_s) values of 28.8, 31.9, and 35.5 emu/g at 10 kOe were observed for the $NiFe_2O_4$/PVP composite nanofibers calcined at 500, 600, and 700 °C, respectively. It is found that the increase of M_s is consistent with the enhancement of crystallinity, and the values of M_s for the $NiFe_2O_4$ samples were observed to increase with increasing crystallite size. It is worth noting that the saturation value of 35.5 emu/g obtained in the sample calcined at 700 °C (crystallite size of 27 nm) was comparable to the values of 34.5 emu/g for $NiFe_2O_4$ nanoparticles (crystallite size of ~68 nm) prepared by egg white solution route [20] and of 34.9 emu/g for carbon coated Ni nanoparticles [44] but lower than the theoretical saturation magnetization of 50 emu/g calculated

using Neel's sublattice theory and the reported value of 56 emu/g for the bulk sample [45]. From Figure 7, the remnant magnetization (M_r) values of 4.4, 4.5, and 6.6 emu/g were observed for the $NiFe_2O_4$/PVP composite nanofibers calcined at 500, 600, and 700 °C, respectively. As a result, the ratio of remnant magnetization to bulk saturation magnetization, M_r/M_s, of the $NiFe_2O_4$/PVP composite nanofibers calcined at 500, 600, and 700 °C were 0.152, 0.141, and 0.188, respectively. These results are not consistent with the results obtained on ferromagnetic nanoparticles reported in literature [20,46]. For ferromagnetic nanoparticles, it is interesting to note that the magnetization is strongly dependent on their particle size, as shown by electron holography study of carbon-coated Ni and Co nanoparticles [46]. The ratio of remnant magnetization to bulk saturation magnetization, M_r/M_s, of Co decreased from 53% to 16% and of Ni decreased from 70% to 30% as the particle diameter increased from 25 to 90 nm. In the case of $NiFe_2O_4$ nanoparticles synthesized by egg white solution method [20], the ratio of M_r/M_s decreased from 14.8% to 3.8% as the particle diameter increased from 54 to 107 nm. It is clearly seen from these two reports that the smaller the particles the higher the remnant magnetization. This is due to the tendency of smaller particles to be a single magnetic domain while larger particles usually contain multiple domains. At present, we cannot explain the difference in the M_r/M_s values obtained in our calcined $NiFe_2O_4$/PVP composite nanofibers. However, it is possible that magnetic anisotropy may play an important role and further work is needed to achieve thorough understanding.

The coercive forces (H_c) were obtained to be 130.5, 114.0, and 138.5 Oe for the $NiFe_2O_4$/PVP composite nanofibers calcined at 500, 600, and 700 °C, respectively. These values are comparable to the value of 130 Oe for the sol-gel synthesized $NiFe_2O_4$ nanoparticles (crystallite size of 16-20 nm) and are higher than the value of 30 Oe for the electrospun $NiFe_2O_4$ nanofibers calcined at 550 °C (crystallite size of 13-16 nm, fiber diameter of 46 ± 9 nm), reported by Li *et al.* [36]. It is seen from the present study that the H_c values of the calcined $NiFe_2O_4$/PVP composite nanofibers do not change much with crystallite size. This is quite different from the case of egg white solution-synthesized $NiFe_2O_4$ nanoparticles that value of coercivity decreases with increasing crystallite size. In this case, the variation of H_c with particle size can be explained on the basis of domain structure, critical diameter and the anisotropy of the crystal [47–49]. A crystallite will spontaneously break up into a number of domains in order to reduce the large magnetization energy it would have if it were a single domain. Thus, coercivity of magnetic particles decreases with particle size once the dimension has dropped below the radius (r_c) of a single magnetic domain and for $NiFe_2O_4$, this parameter is close to 100 nm [50]. Recently, Kinemuchi *et al.* [15] reported that superparamagnetism appears at 27 °C (300 K) if the particle size of $NiFe_2O_4$ falls below 20 nm. Since the size of particles in our samples (9, 21, and 27 nm) was very close to this value, it is believed that the coercivities of our samples should be determined mainly by the portion of particles with crystallite sizes larger than 20 nm. The values of specific magnetization at 10 kOe, remnant magnetization (M_r), the ratio of remnant magnetization to bulk saturation magnetization (M_r/M_s), and the coercive forces (H_C) are also tabulated in Table 1.

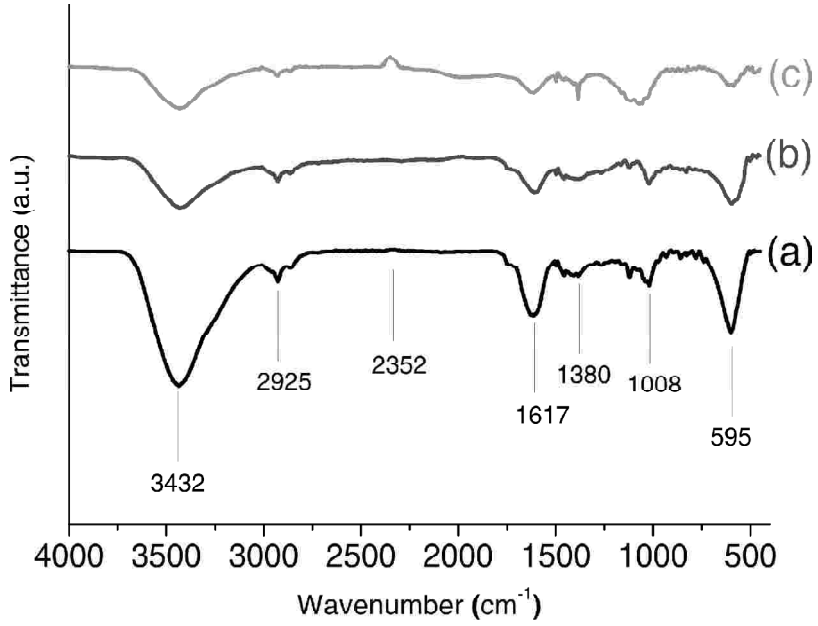

Figure 6: FT-IR Spectra of the $NiFe_2O_4$/PVP Composite Samples Calcined in Air for 3 h at Different Temperatures. (a) 500 °C, (b) 600 °C, and (c) 700 °C

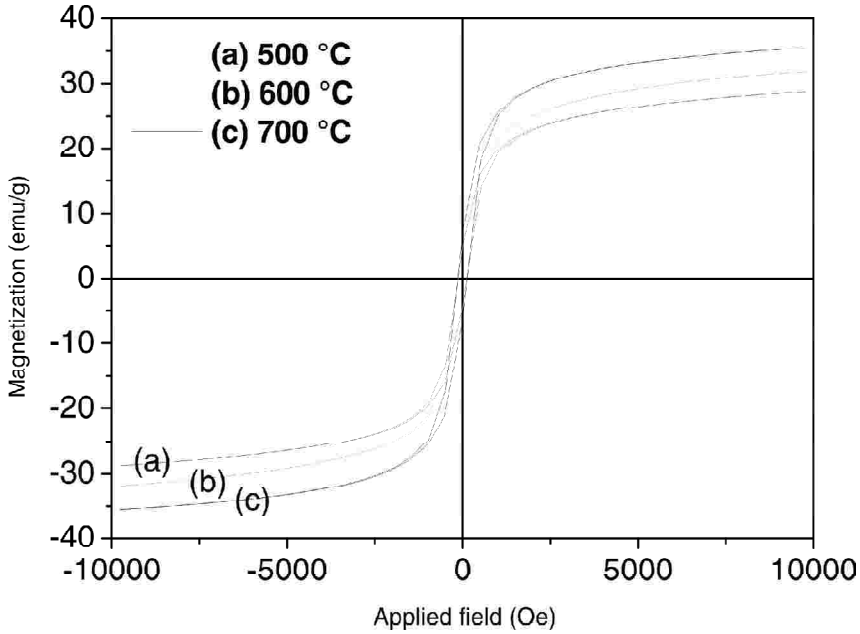

Figure 7: The Specific Magnetization of the $NiFe_2O_4$/PVP Composite Samples Calcined in air for 3 h at Different Temperatures, as a Function of Field, Measured at 20 °C. (a) 500 °C, (b) 600 °C, and (c) 700 °C.

4. CONCLUSION

Nanofibers of $NiFe_2O_4$ have been successfully fabricated using an electrospinning technique. Polycrystalline $NiFe_2O_4$ nanofibers (diameter of ~160-200 nm) as confirmed by XRD, FT-IR and SAED were formed after calcination of the as-spun $NiFe_2O_4$/PVP composite nanofibres in air at above 500 °C for 3 h. The nanofibers consisted of the structure of packed particles or crystallites of ~ 10-80 nm, as revealed by TEM. The crystal structure and morphology of the nanofibers were influenced by the calcination temperature. All of the electrospun $NiFe_2O_4$ samples are ferromagnetic, having their hysteresis loop in the range of -2000 Oe < H < 2000 Oe with the specific magnetizations of 28.8, 31.9, and 35.5 emu/g at 10 kOe for the samples calcined at 500, 600, and 700 °C , respectively. We believe that the electrospun $NiFe_2O_4$ nanofibers could have potential in some new applications as ferromagnetic fibers for nanocomposites, separation, anodic material in lithium ion batteries, catalyst, and as electronic material for nanodevices and storage devices.

ACKNOWLEDGEMENT

The authors would like to thank the Department of Chemistry for providing TG-DTA, FTIR and VSM facilities, the Science and Technology Service Center (Chiang Mai University) for providing TEM facilities, and the Department of Physics, Faculty of Science, Ubon Ratchathani University for providing XRD facilities, and the Thai Microelectronics Center (TMEC) for FE-SEM facilities. This work is partially supported by The National Nanotechnology Center (NANOTEC), NSTDA, Ministry of Science and Technology, Thailand, through its program of Center of Excellence.

References

[1] R. Valenzuela, Magnetic Ceramics, Cambridge University Press, Cambridge, 1994.

[2] M. H. Sousa, E. Hasmonay, J. Depeyrot, F. A. Tourinho, J. C. Bacri, E. Dubois, R. Perzynski, and Yu. L. Raikherb, J. Magn. Magn. Mater. **242**, (2002), 572.

[3] S. Bae, S. W. Lee, Y. Takemura, *Appl. Phys. Lett.* **89**, (2006), 252-503.

[4] C. G. Ramankutty, S. Sugunan, *Appl. Catal. A.* **218**, (2001), 39.

[5] V. Sepelak, D. Baabe, D. Mienert, D. Schultze, F. Krumeich, F. J. Litterst, and K. D. Becker, *J. Magn. Magn. Mater.* **257**, (2003), 377.

[6] N. Rezlescu, N. Iftimie, E. Rezlescu, C. Doroftei, P. D. Popa, Sensors and Actuators B 114 (2006), 427.

[7] S. Rana, A. Gallo, R. S. Srivastava, R. D. K. Misra, Acta Biomater. **3**, (2007), 233.

[8] H. Zhao, Z. Zheng, K. W. Wong, S. Wang, B. Huang, D. Li, Electrochem. Comm. **9**, (2007), 2606.

[9] I. Safarik, M. Safarikova, Magnetic Nanoparticles and Biosciences, In Nanostructured Materials, edited by H. Hofmann, Z. Rahman, U. Schubert, Springer, Wien, 2002, pp. 1–23.

[10] K. V. P. M. Shafi, Y. Koltypin, A. Gedanken, R. Prozorov, J. Balogh, J. Lendavi, I. Felner, *J. Phys. Chem. B* 101, (1997), 6409.

[11] S. Prasad, N. S. Gajbhiye, *J. Alloys Compd.* **265**, (1998), 87.

[12] J. M. Yang, W. J. Tsuo, F. S. Yen, *J. Solid State Chem.* **145**, (1999), 50.

[13] Y. Shi, J. Ding, X. Liu, J. Wang, *J. Magn. Magn. Mater.* **205**, (1999), 249.

[14] D. H. Chen, X. R. He, Mater. *Res. Bull.* **36**, (2001), 1369.

[15] Y. Kinemuchi, K. Ishizaka, H. Suematsu, W. Jiang, K. Yatsui, Thin Solid Films **407**, (2002), 109.

[16] J. Liu, H. He, X. Jin, Z. Hao, Z. Hu, *Mater. Res. Bull.* **36**, (2001), 2357.

[17] A. Kale, S. Gubbala, R. D. K. Misra, *J. Magn. Magn. Mater.* **277**, (2004), 350.

[18] J. Zhou, J. Ma, C. Sun, L. Xie, Z. Zhao, H. Tian, *J. Am. Ceram. Soc.* **88**, (2005), 3535.

[19] P. E. Meskin, V. K. Ivanov, A. E. Barantchikov, B. R. Churagulov, Y. D. Tretyakov, Ultrason. Sonochem. **13**, (2006), 47.

[20] S. Maensiri, C. Masingboon, B. Boonchom, S. Seraphin, *Scripta Mater.* **56**, (2006), 797.

[21] Z. H. Hua, R. S. Chen, C. L. Li, S. G. Yang, M. Lu, B. X. Gu, Y. W. Du, *J. Alloys Compd.* **427**, (2007), 199.

[22] G. Ji, S. Tang, B. Xu, B. Gu, Y. Du, *Chem. Phys. Lett.* **379**, (2003), 484.

[23] D. H. Renaker, I. Chun, Nanotechnology, **7**, (1996), 216.

[24] A. Frenot, I. S. Chronakis, Curr. Opin. Colloid. *Inter. Sci.* **8**, (2003), 64.

[25] Z. H. Huang, Y. Z. Zhang, M. Kotaki, S. Ramakrishna, *Comp. Sci. Tech.* **63**, (2003), 2223.

[26] D. Li, Y. Xia, *Adv. Mater.* **16**, (2004), 1151.

[27] D. H. Reneker, A. L. Yarin, H. Fong, S. Koombhonge, *J. Appl. Phys.* **87**, (2000), 4531.

[28] A. L. Yarin, S. Koombhongse, D. H. Reneker, *J. Appl. Phys.* **89**, (2001), 3018.

[29] A. L. Yarin, D. H. Reneker, *J. Appl. Phys.* **90**, (2001), 4836.

[30] G. C. Rutledge, S. V. Fridrikh, *Adv. Drug Delivery Rev.* **59**, (2007), 1384.

[31] S. Naunsing, S. Ninmuang, W. Jarernboon, S. Maensiri, S. Seraphin, Mater. Sci. Eng. B **131**, (2006), 147.

[32] P. Viswanathamurthi, N. Bhattarai, H. Y. Kim, D. R. Lee, Nanotechnology **15**, (2004), 320.

[33] Y. Wang, J. J. Santiago-Aviles, *Nanotechnology*, **15**, (2004), 32.

[34] S. Maensiri, W. Nuansing, *Mater. Chem. Phys.*, **99**, (2006), 104.

[35] S. Maensiri, W. Nuansing, J. Klinkaewnarong, P. Laokul, J. Khemprasit, *J. Colloid Interf. Sci.* **297**, (2006), 578.

[36] D. Li, T. Herricks, Y. Xia, *Appl. Phys. Lett.*, **83**, (2003), 4586.

[37] B. D. Cullity, S. R. Stock, Elements of X-ray Diffraction, Prentice Hall, Englewood Cliffs, 2001.

[38] A. A. Kamnev, M. Risti, *J. Mol. Struct.*, **408/409**, (1997), 301.

[39] D. Chen, D. Chen, X. Jiao, Y. Zhao, M. He, *Powder Technology*, **133**, (2003), 247.

[40] M. Mouallem-Bahout, S. Bertrand, O. Pena, *J. Solid Sate Chem.*, **178**, (2005), 1080.

[41] V. A. M. Brabers, *Phys. Stat. Sol.*, **33**, (1969), 563.

[42] S. Hafner, Z. Krist., **115**, (1961), 331.

[43] R. D. Waldron, *Phys. Rev.*, **99**, (1955), 1727.

[44] J. Jiao, S. Seraphin, X. Wang, J. C. Withers, *J. Appl. Phys.* **80**, (1996) 1.

[45] V. Sepelak, K. Tkacova, V. V. Boldyrev, S. Wibmann, K. D. Becker, *Physica B.* **617**, (1997), 234.

[46] S. Seraphin, C. Beeli, J. M. Bonard, J. Jiao, P. A. Stadelmann, A. Chatelain, *J. Mater. Res.*, **14**, (1999), 2861.

[47] B. D. Cullity, Introduction to Magnetic Materials, Addison-Wesley Publishing Company. Inc, Reading, MA, 1972.

[48] S. Chikazumi, Physics of Magnetism, Wiley, New York, 1959.

[49] M. Georgea, A. Mary John, S. S. Naira, P. A. Joy, M. R. Anantharaman, *J. Magn. Magn. Mater.*, **302**, (2006), 190.

[50] I. S. Jacobs, C. P. Bean, *Phys. Rev.* **100**, (1955), 1060.

List of Figure Captions